Available online at www.sciencedirect.com
SCIENCE DIRECT®
Journal of Magnetic Resonance 180 (2006) 137–146
JMR Journal of Magnetic Resonance
www.elsevier.com/locate/jmr

Isotope selection in distance measurements between nitroxides

G. Jeschke [a,*], H. Zimmermann [b], A. Godt [c]

[a] Max Planck Institute for Polymer Research, Postfach 3148, 55021 Mainz, Germany
[b] Max Planck Institute for Medical Research, Jahnstrase 29, 69120 Heidelberg, Germany
[c] Universität Bielefeld, Fakultät für Chemie, Universitätsstrasse 25, 33615 Bielefeld, Germany

Received 18 November 2005; revised 13 January 2006
Available online 21 February 2006

Abstract

Self-assembly of spin-labeled synthetic macromolecules or biomacromolecules can lead to structures that contain more than two nitroxide radicals. Label-to-label distance distributions are then poorly resolved since established electron paramagnetic resonance techniques for distance measurements cannot select between the different pairs of nitroxides. A separation into different contributions can be achieved by partially labeling the nitroxide radicals by ^{15}N or by deuterium and applying pulse electron electron double resonance techniques. With ^{15}N labeling, strong suppression of either the ^{14}N or the ^{15}N contribution can be achieved by suitable choices of the excitation bandwidths and frequencies of the observer subsequence and pump pulse and linear combination of data sets. With deuterium labeling, interactions between only the isotope-labeled nitroxides can be selected by a two-dimensional version of the four-pulse double electron electron resonance experiment. This selection is based on the deep electron spin echo envelope modulation of deuterated nitroxides.

Keywords: EPR; ELDOR; Spin labeling; Protein structure; ESEEM

1. Introduction

Recently developed techniques for measuring long distances between two nitroxide radicals [1–7] have strongly contributed to a renewed interest in spin-labeling of biomacromolecules [8–11] and synthetic macromolecules [12,13]. These techniques are well suited for characterizing the structure and structural changes of isolated doubly labeled macromolecules. As distance distributions can be extracted from the data [14–17], this applies even in cases where a protein can adopt distinct conformations [18] or where a synthetic macromolecule samples a broad conformational ensemble [19]. The situation becomes more complicated when the macromolecules interact strongly with each other. For homodimers [20] and homotrimers [18] of membrane proteins, distance distributions can still be interpreted with some confidence, but they may be poorly resolved and difficult to assign for larger assemblies, in particular, if these assemblies consist of more than one type of macromolecules. Such complexes of several different macromolecules are the functional units in many biochemical processes [21] and may also be encountered in self-assembling synthetic materials. Investigation of their structure and structural dynamics by spin-labeling techniques requires methods for selective distance measurements in systems containing more than two nitroxide radicals. In principle, one could separately prepare and measure distance distributions A–A and B–B on systems, in which only one of the components A or B is labeled, and subtract them from the distance distribution of the system in which both components A and B are labeled. However, this approach is reliable only if the system can be prepared with precisely known concentrations and degrees of labeling of both components. For biomacromolecules, it is often difficult—and sometimes impossible—to meet these requirements and verify that they are met. An experimental technique for

* Corresponding author. Fax: +49 6131 379 100.
E-mail address: jeschke@mpip-mainz.mpg.de (G. Jeschke).

1090-7807/$ - see front matter © 2006 Elsevier Inc. All rights reserved.
doi:10.1016/j.jmr.2006.02.002

separating the distance distributions in data obtained from a sample in which both components are labeled, would thus be useful.

The self-assembly of these systems from different macromolecules makes it simple to introduce chemically different nitroxide labels as a basis for such selective distance measurements. However, the electron paramagnetic resonance (EPR) spectra change only slightly with changes in nitroxide structure, so that EPR spectra of different nitroxides in general overlap strongly. Selective distance measurements may thus require a judicious choice of the different nitroxides as well as an optimized experimental approach. In this work, we consider isotope labeling as a means for distinguishing between the nitroxides and the four-pulse double electron electron resonance (DEER) experiment [5,7,22] as the basis for the selective distance measurements. As a first approach, we examine ^{15}N labeling, which introduces a strong change in the nitroxide EPR spectrum, in conjunction with a spectral selection technique that was previously used to distinguish between nitroxide–nitroxide and nitroxide–copper pairs [23]. This technique might be adapted to the three-pulse electron electron double resonance (PELDOR) experiment [1,2,12]. As a second approach, we investigate selective measurements of the distance between perdeuterated spin labels by using nuclear-modulation filtering. This technique might be adapted to double-quantum EPR [4]. Both approaches are demonstrated on mixtures of a 2.8 nm long isotope-labeled shape-persistent biradical with a 3.7 nm long non-labeled biradical.

The paper is organized as follows. First, we consider the efficiency of spectral selection in four-pulse DEER on a mixture of ^{14}N and ^{15}N labeled nitroxides. For this, numerical simulations of the excitation profiles of the observer sequence and the pump pulse are performed and the excitation profiles are then used to compute the selection efficiencies for different combinations of observer and pump positions in the spectrum. Second, we test the selection efficiency by a series of experiments on the mixture of biradicals. Third, we discuss the electron spin echo envelope modulation (ESEEM) effect introduced into four-pulse DEER by variation of the first interpulse delay. We describe a procedure for extracting a one-dimensional deuterium-filtered DEER trace from the two-dimensional data set obtained in such an experiment and test this procedure on experimental data. We conclude with a short discussion of the comparative advantages and disadvantages of the two approaches.

2. Materials and methods

2.1. Model systems

Synthesis of the shape-persistent biradicals (Fig. 1) with end-to-end distances of approximately 2.8 (**1**) and 3.7 nm (**2**) has been described earlier [5,24]. The isotope-labeled biradicals were obtained by replacing 1-oxyl-2,2,5,5-tetramethylpyrroline-3-carboxylic acid (**3**) with natural isotope abundance by perdeuterated **3** or perdeuterated and additionally ^{15}N-labeled **3**. Mixtures of 0.1 g of an isotope-labeled biradical **1** and 0.1 g of the radical **2** were dissolved in 400 mg molten *o*-terphenyl (Aldrich) for nuclear modulation filtered DEER and in perdeuterated *o*-terphenyl for spectral selection experiments. Using a perdeuterated matrix is not mandatory for these experiments, but improves resolution of the distance distribution [7]. The crystallized mixtures were powdered, filled into home-made 3 mm o.d. Herasil EPR tubes, remolten with a heat gun adjusted to 100 °C air temperature, and shock-frozen by immersing the sample tube into liquid nitrogen. Shock-frozen samples were immediately transferred into the EPR probehead that was pre-cooled to 80 K.

2.2. EPR measurements

All experiments were performed at X-band frequencies (9.3–9.4 GHz) with a Bruker Elexsys 580 spectrometer equipped with a Bruker Flexline split-ring resonator ER

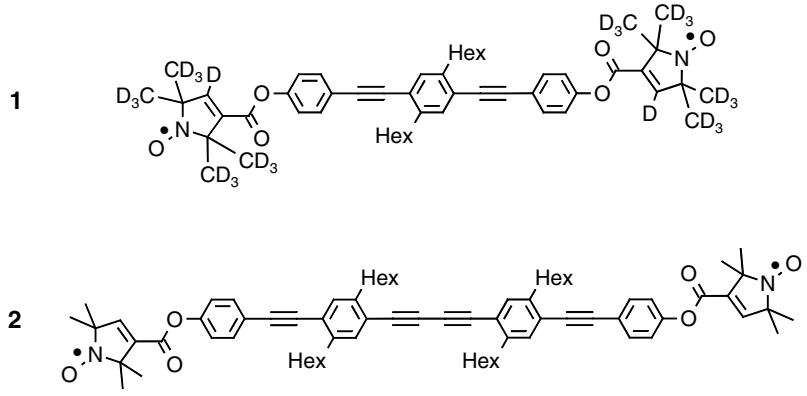

Fig. 1. Structures of the shape-persistent biradicals used as model compounds. Biradical **1** with a nitroxide–nitroxide distance of 2.8 nm is used with ^{15}N labeling of both nitroxides in the spectral selection experiments and with natural abundance (^{14}N) nitroxides in the nuclear-modulation filtered experiment. Biradical **2** with a nitroxide–nitroxide distance of 3.7 nm is used without any isotope-labeling in both types of experiments.

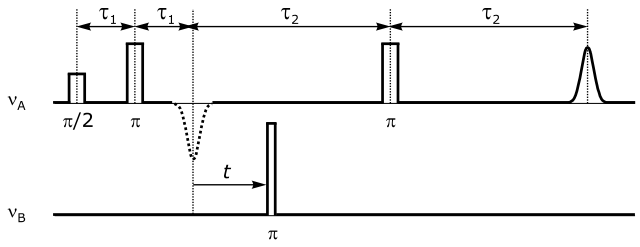

Fig. 2. Four-pulse DEER sequence consisting of an observer subsequence (refocused Hahn echo) with fixed interpulse delays on frequency ν_A and a pump pulse on frequency ν_B positioned at a variable delay t' with respect to the first Hahn echo. In the two-dimensional nuclear modulation filtered experiment, delay τ_1 is varied in the second dimension.

4118X_MS3. Microwave from a YIG oscillator (Avantek AV 78012) customized by Magnettech GmbH Berlin was fed into one microwave pulse forming unit of the spectrometer to provide the pump pulses. All measurements were performed using the four-pulse DEER experiment $\pi/2(\nu_A)$–τ_1–$\pi(\nu_A)$–t'–$\pi(\nu_B)$–$(\tau_1+\tau_2-t')$–$\pi(\nu_A)$–τ_2–echo (Fig. 2) [5]. For spectral selection experiments, time t' was varied, while times τ_1 and τ_2 were kept constant. For nuclear modulation filtered DEER, times t' and τ_1 were varied to obtain a two-dimensional data set. In all experiments, the resonator was overcoupled to $Q \approx 100$ and the pump frequency ν_B was set to the center of the resonator dip. For nuclear-modulation filtered DEER the pump frequency coincided with the maximum of the nitroxide EPR spectrum, while the observer frequency ν_A was 65 MHz higher and coincided with the low-field local maximum of the spectrum. The pump and observer positions for spectral selection experiments are explained below. All measurements were performed at a temperature of 80 K with observer pulse lengths of 32 ns for both $\pi/2$ and π pulses. A pump pulse length of 12 ns was used for nuclear-modulation filtered DEER and a pump pulse length of 24 ns for spectral selection. In spectral selection experiments, proton modulation was averaged by adding traces at eight different τ_1 values, starting at $\tau_1(0) = 400$ ns and using an increment of 8 ns. Data sets with 760 points were acquired using an increment of 8 ns and a starting value of -328 ns for t'. The measurement time for each experiment was approximately 2 h. In the nuclear modulation filtered experiment, τ_1 was incremented in steps of 16 ns starting at 200 ns for a total of 128 traces, while t' was incremented in steps of 8 ns starting at $t' = -128$ ns for a total of 500 data points per trace. The measurement time for this experiment was 14 h.

2.3. Data analysis

Background correction was performed and distance distributions were computed with the Matlab program DeerAnalysis 2004 [25] and based on algorithms described in Ref. [15]. Tikhonov regularization in distance domain with a regularization parameter of 0.5 was used for all data sets. Nuclear-modulation filtering was performed with a home-written Matlab program based on an algorithm that is described below.

3. Selectivity of detection and pumping in four-pulse DEER

3.1. General considerations

The four-pulse DEER experiment detects the dipole–dipole interaction between an observer spin A and a pumped spin B as a modulation of a refocused Hahn echo (Fig. 2). Due to the limited excitation bandwidth of the observer subsequence only a fraction f_A of the paramagnetic centers acts as observer spins A. Likewise, only a fraction f_B of the spins is pumped, since the excitation bandwidth of the pump pulse is typically also narrower than the EPR spectrum. The fractions f_A and f_B depend mainly on the lengths and flip angles of the pulses, on the EPR lineshape, and on the observer and pump positions in the spectrum. In addition, the fractions are influenced by the microwave (m.w.) pulse shape, which in turn depends on the rise and fall time of the PIN diode switches used for pulse forming, on resonator bandwidth, shape of the m.w. mode, and position of the observer frequency ν_A and pump frequency ν_B with respect to the center of the mode. For simplicity, we assume rectangular pulses and infinite resonator bandwidth in the following model computations. This approximation is sufficient for a semi-quantitative understanding of spectral selection effects. Due to pulse imperfections experimental fractions f_A and f_B will be slightly smaller than computed ones.

For distances shorter than 2 nm, fractions f_A and f_B also depend on the dipole–dipole coupling itself, as this coupling is then of the same order of magnitude as typical excitation bandwidths of m.w. pulses. For distances shorter than 1.75 nm, the coupling is comparable to the difference of the resonance frequencies of A and B spins. Generally, numerical computations should thus be performed with the static Hamiltonian [6]

$$\hat{H}_0 = \Omega_A \hat{S}_{z,A} + \Omega_B \hat{S}_{z,B} + \omega_{dd} \hat{S}_{z,A} \hat{S}_{z,B} - \frac{\omega_{dd}}{2} (\hat{S}_{x,A} \hat{S}_{x,B} + \hat{S}_{y,A} \hat{S}_{y,B}), \quad (1)$$

where Ω_A and Ω_B are the resonance offsets of A and B spins, respectively, and ω_{dd} is the dipole–dipole coupling.

Model computations in this work are performed with the Hamiltonian given in Eq. (1), using $\omega_{dd}/(2\pi) = 2$ MHz and $\Omega_A - \Omega_B = 65$ MHz. During pulses, the Hamiltonian is given by $\hat{H}_0 + \hat{H}_1$, where $\hat{H}_1 = \omega_1 \hat{S}_{x,A}$ for the observer sequence and $\hat{H}_1 = \omega_1 \hat{S}_{x,B}$ for the pump pulse. The m.w. field strength is given by $\omega_1 = \pi/(t_p)$, where t_p is the length of a π pulse. We have checked that the results are representative for cases where all distances are longer than 2 nm. At shorter distances, quantitative computations would require an integration over all possible differences $\Omega_A - \Omega_B$, taking into account the EPR lineshape and excitation of both spins by both observer and pump

pulses. Here, we refrain from such time-consuming computations for this range of short distances. Computations were performed by home-written Matlab programs that implement density formalism.

3.2. Observer subsequence

The fraction of observed spins can be computed from the normalized excitation profile $p_A(\Omega)$ of the observer sequence and the spectral lineshape of the nitroxide $I(\Omega)$,

$$f_A = \frac{\int p_A(\Omega) I(\Omega)\,d\Omega}{\int I(\Omega)\,d\Omega}. \quad (2)$$

The excitation profile $p_A(\Omega)$ in turn is obtained by computing the echo intensity as a function of Ω_A. In this computation, the density matrix at time zero before the first observer pulse $\sigma_{0,A} = -\hat{S}_{z,A}$ does not depend on Ω_A. We performed such computations for the pulse sequence shown in Fig. 2 with $\tau_1 = 200$ ns and $\tau_2 = 1200$ ns. The signal intensity was computed as the expectation value of $\hat{S}_{y,A}$ at time increments of 4 ns starting 16 ns before the center of the refocused echo and ending 16 ns after refocused echo. The sum of the signal intensities at these data points was taken to account for echo integration in the experiment.

For a length of 32 ns of all observer pulses, as used in our experiments, we obtain the excitation profile shown as a dotted line in Fig. 3. This profile can be fitted quite well by a Gaussian distribution with a standard deviation of 10 MHz, corresponding to a full width at half height of 16 MHz or 0.57 mT. For the situation shown in Fig. 3 for a ^{14}N nitroxide we find $f_A = 0.106$. If the observer position is set to the maximum of the nitroxide spectrum (compare position P_5 in Fig. 4), we find $f_A = 0.178$. If observer efficiency is maximized for a ^{15}N nitroxide, corresponding to position P_4 in Fig. 4), we have $f_A = 0.209$.

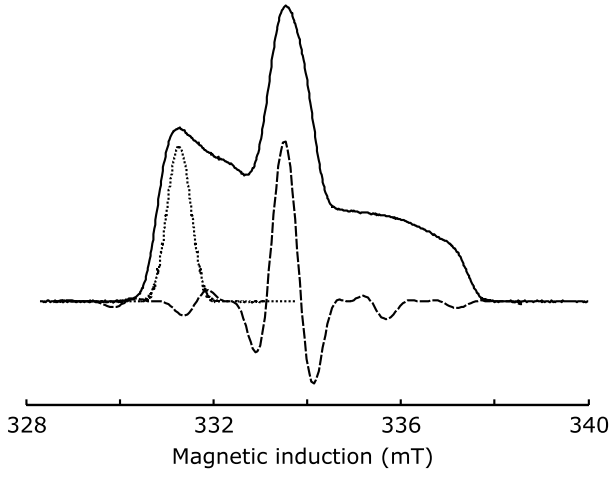

Fig. 3. EPR spectrum of a ^{14}N nitroxide (solid line) and computed excitation profiles of the observer sequence with pulse lengths of 32 ns (dotted line) and of a pump pulse with a length of 12 ns (dashed line). The positions of the pump and observer correspond to the situation in nuclear-modulation filtered DEER; they can be shifted to change spectral selection.

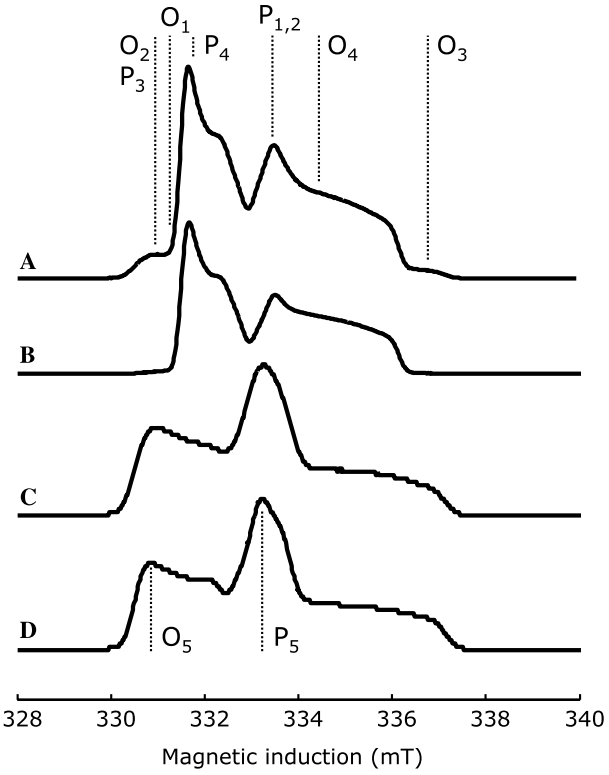

Fig. 4. Pump positions P_i and observer positions O_i for ^{14}N versus ^{15}N isotope selection. (A) Echo-detected EPR spectrum of the mixture of ^{15}N labeled biradical **1** and natural abundance (99.63% ^{14}N) biradical **2** with pump and observer positions for isotope-selective DEER. (B) Echo-detected EPR spectrum of ^{15}N labeled biradical **1**. (C) Echo-detected EPR spectrum of natural abundance biradical **2**. (D) Echo-detected EPR spectrum of the mixture of deuterated biradical **1** with natural abundance of nitrogen isotopes and natural abundance (99.91% ^{1}H) biradical **2** with pump and observer positions for nuclear modulation filtered DEER.

3.3. Pump pulse

To calculate pump pulse efficiency, we have to consider the required coherence transfer $\hat{S}_{x,A}\hat{S}^{\alpha}_{B} \leftrightarrow \hat{S}_{x,A}\hat{S}^{\beta}_{B}$. Hence we apply the pulse of length t_p to an initial density matrix $\hat{S}_{x,A}\hat{S}^{z}_{B}$. To correct for the evolution of electron coherence on observer spin A that would also occur in the absence of the pulse, we then apply the Hamiltonian $\hat{H}_{corr} = -\Omega_A \hat{S}_{z,A}$ for a time t_p before computing the expectation value of $\hat{S}_{x,A}\hat{S}^{\beta}_{B}$. For $t_p = 24$ ns, we thus obtain the excitation profile shown as a dashed line in Fig. 3. For $t_p = 32$ ns and pump position P_5 in Fig. 4, we find $f_B = 0.273$ for a ^{14}N nitroxide. Experimental values for this pulse length are $f_B \approx 0.30$. For $t_p = 12$ ns and the same pump position, we find $f_B = 0.489$ for a ^{14}N nitroxide, while the experimental value is $f_B \approx 0.43$. In the latter case, experimental imperfections of the pulse flanks may play a role. Nevertheless, we consider the agreement between these relatively simple simulations and experiments as quite good. For ^{14}N nitroxides with our typical experimental settings (32 ns observer pulses, 12 ns pump pulse), the computations suggest that the dipolar modulation in four-pulse DEER corresponds to 5% of the total EPR signal of all

spins. This estimate is one order of magnitude larger than the one presented in a previous theoretical comparison of double-quantum techniques with DEER [26].

4. ^{14}N versus ^{15}N isotope selection via the pump and observer position

4.1. Theoretical predictions

To quantify the expected isotope selection, we may define a suppression factor F_{suppr} for the unwanted contribution. In an experiment intended to detect the ^{14}N contribution and suppress the ^{15}N contribution, this factor is given by

$$F_{\mathrm{suppr}}(^{15}\mathrm{N}) = \frac{f_{\mathrm{A}}(^{15}\mathrm{N}) f_{\mathrm{B}}(^{15}\mathrm{N})}{f_{\mathrm{A}}(^{14}\mathrm{N}) f_{\mathrm{B}}(^{14}\mathrm{N})}, \tag{3}$$

where f_{A} and f_{B} depend on the selected observer and pump position, respectively. In an experiment intended to detect the ^{15}N contribution and suppress the ^{14}N contribution, the factor is

$$F_{\mathrm{suppr}}(^{14}\mathrm{N}) = \frac{1}{F_{\mathrm{suppr}}(^{15}\mathrm{N})}. \tag{4}$$

Using the pump and observer positions P_1 and O_1 indicated in Fig. 4A, we find $F_{\mathrm{suppr}}(^{15}\mathrm{N}) = 0.46$, i.e., only a slight differentiation between the two isotopes. Keeping the pump position $P_2 = P_1$ but changing the observer position to O_2 gives $F_{\mathrm{suppr}}(^{15}\mathrm{N}) = 0.083$, i.e., a substantial suppression of the ^{15}N contribution. An even better suppression is expected when selecting both the pump and observer position outside the ^{15}N nitroxide spectrum (positions P_3 and O_3). Here, we find $F_{\mathrm{suppr}}(^{15}\mathrm{N}) = 0.023$. In other words, for an equimolar mixture of ^{14}N and ^{15}N biradicals, the spectral contribution due to the ^{15}N biradicals should be as small as 2.3%.

This suppression comes at the expense of sensitivity in detecting the wanted contribution. The signal-to-noise ratio for the ^{14}N contribution is proportional to $f_{\mathrm{A}}(^{14}N) f_{\mathrm{B}}(^{14}\mathrm{N})$. If we normalize sensitivity for pump and observer positions P_1 and O_1 to unity, we find that the sensitivity is only 64% for positions P_2/O_2 and only 19% for positions P_3/O_3. The latter choice may thus be useful only for samples with a relatively strong signal.

The ^{14}N contribution cannot be suppressed that strongly, as the ^{14}N nitroxide spectrum completely overlaps the ^{15}N nitroxide spectrum. Nevertheless, relative suppression of the ^{14}N contribution is expected when the pump and observer positions correspond to significantly higher spectral intensity in the ^{15}N nitroxide spectrum compared to the ^{14}N nitroxide spectrum. The optimum choice for this is close to positions P_4 and O_4. Here, we find a suppression factor $F_{\mathrm{suppr}}(^{14}\mathrm{N}) = 0.44$. Compared to the optimum conditions for detecting the ^{15}N contribution (pump position P_4, observer position coinciding with P_1), the sensitivity loss is moderate: the signal-to-noise ratio should still correspond to 88% of the optimum one. While a direct selective detection of the ^{15}N contribution is impossible with this suppression factor, it is feasible to extract both contributions by linear combination of the data sets from two DEER experiments with different ^{14}N suppression factors. The DEER signal for each experiment is given by

$$V(t) = \frac{F_{\mathrm{suppr}}(^{14}\mathrm{N})}{1 + F_{\mathrm{suppr}}(^{14}\mathrm{N})} V_{^{14}\mathrm{N}}(t) + \frac{1}{1 + F_{\mathrm{suppr}}(^{14}\mathrm{N})} V_{^{15}\mathrm{N}}(t). \tag{5}$$

Let the two suppression factors be F_1 and F_2 and the two DEER signals V_1 and V_2. The pure contributions are then given by:

$$V_{^{14}\mathrm{N}} = \frac{(1 + F_1)V_1 - (1 + F_2)V_2}{F_1 - F_2} \tag{6}$$

and

$$V_{^{15}\mathrm{N}} = \frac{F_1 V_2 - F_2(V_1 + F_1(V_1 - V_2))}{F_1 - F_2}. \tag{7}$$

4.2. Experimental results

As predicted in the previous section, time-domain DEER data and dipolar spectra for a mixture of ^{15}N labeled and natural abundance nitroxide biradicals depend strongly on the choice of pump and observer position (Fig. 5). At positions P_1/O_1 both dipolar frequencies are clearly visible in the time-domain data and dipolar spectrum, whereas at positions P_2/O_2 the contribution due to the shorter ^{15}N labeled biradical **1** is barely visible in the time-domain data but still noticeable in the dipolar spectrum. At positions P_3/O_3, this contribution is virtually completely suppressed. In contrast, at positions P_4/O_4 the contribution from the shorter ^{15}N labeled biradical **1** dominates. However, the partially suppressed contribution from the longer natural abundance biradical **2** is still clearly visible in the dipolar spectrum (arrows in bottom trace of Fig. 5B), again in agreement with expectations. The suppression effects are also clearly visible in the distance distributions obtained from the time-domain data by Tikhonov regularization with a regularization parameter of 0.5 after exponential background correction (Fig. 6). This data analysis technique leads to total suppression of the contribution from biradical **1** at positions P_3/O_3 (Fig. 6).

By applying the separation procedure based on Eqs. (6) and (7) to the two data sets obtained at positions P_1/O_1 and P_4/O_4 (Fig. 7A), we obtain not as good a suppression of the ^{15}N contribution as by direct measurement at positions P_3/O_3. This is not surprising, as position P_4/O_4 is specifically selected to enhance the ^{15}N contribution rather than suppress it. Therefore, the

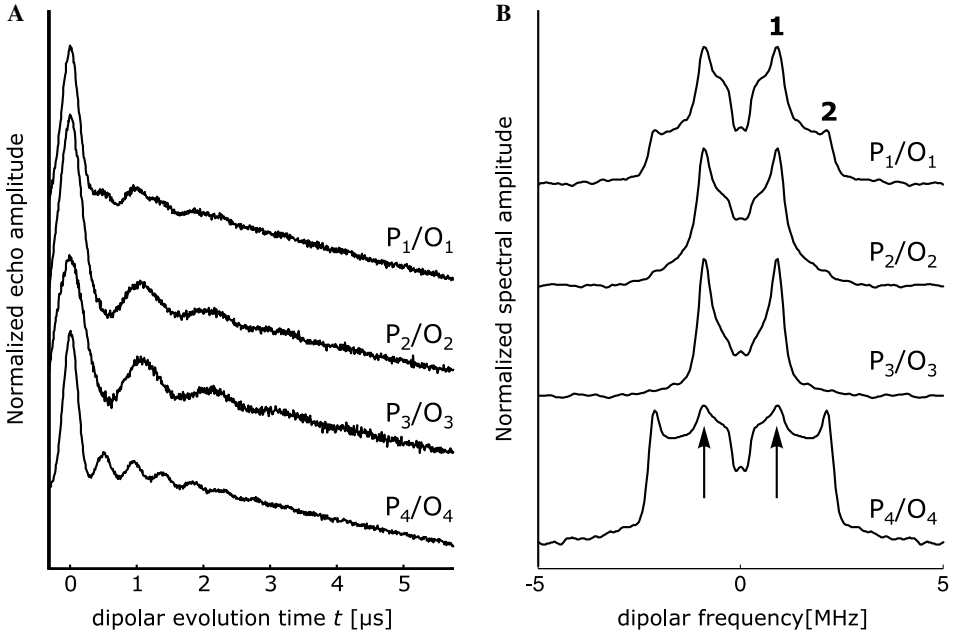

Fig. 5. Time-domain four-pulse DEER data (A) and dipolar spectra (B) measured on a mixture of ^{15}N labeled biradical **1** and natural abundance nitroxide biradical **2** for different choices of pump position P_i and observer position O_i as indicated in Fig. 4.

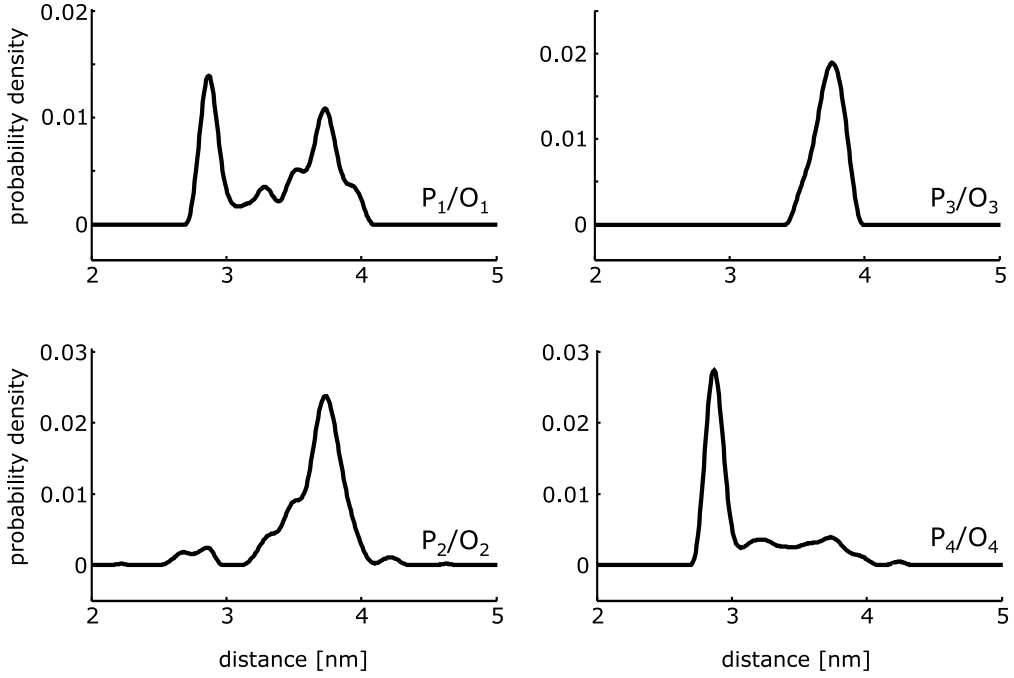

Fig. 6. Distance distributions for a mixture of ^{15}N labeled biradical **1** and natural abundance nitroxide biradical **2** obtained at different choices of pump position P_i and observer position O_i as indicated in Fig. 4.

data trace for biradical **2** obtained from Eq. (6) is rather noisy. Furthermore, ideal suppression cannot be expected as the experimental suppression factors F_{suppr} (^{14}N) and suppression factor F_{suppr} (^{14}N) will somewhat deviate from the theoretical predictions used in the separation. Nevertheless, suppression of the ^{14}N contribution (biradical **2**) is rather good (Fig. 7B). A small contribution from this biradical is still seen in the dipolar spectrum (arrows in the middle trace) and in the distance distribution (bottom trace), but suppression is better than can be achieved in a single measurement at any combination of pump and observer positions. The loss in signal-to-noise ratio compared to the uncorrected measurement at positions P_4/O_4 is significant, yet tolerable.

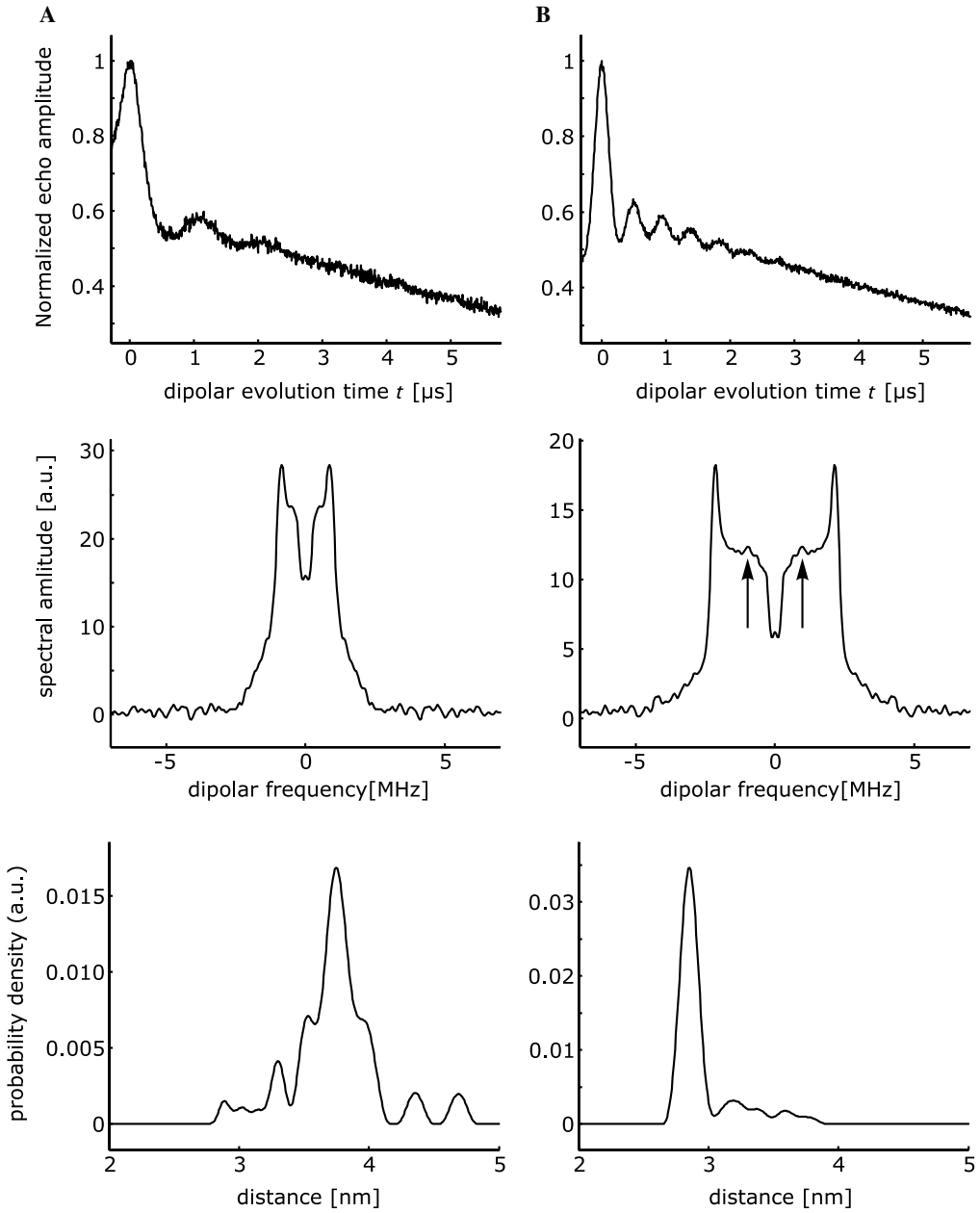

Fig. 7. Isotope selection by linear combination of data sets obtained at different pump and observer positions (P_1/O_1 and P_4/O_4 in Fig. 4, respectively). From top to bottom the separated time-domain data, the corresponding dipolar spectrum, and the distance distribution obtained by Tikhonov regularization are shown. (A) Selection of natural abundance (^{14}N) biradical **2** according to Eq. (6). (B) Selection of ^{15}N labeled biradical **1** according to Eq. (7).

5. Nuclear modulation filtered DEER

5.1. The ESEEM-correlated DEER experiment

In the conventional constant-time, four-pulse DEER experiment with time variable t (see Fig. 2) the dipolar modulation is superimposed by nuclear modulations due to matrix protons or deuterons whose depth depends on specifics of the matrix [5]. This modulation is introduced by excitation of forbidden transitions of the observer spins by the pump pulse. We have previously reported that it can be partially averaged by varying interpulse delay τ_1 and adding the data traces [6,7]. If the traces are recorded separately, such variation of interpulse delay τ_1 introduces nuclear modulation along an additional τ_1 dimension that stems from the action of only the observer pulses on the observer spins. This is because the subsequence $\pi/2(\nu_A)$–τ_1– $\pi(\nu_A)$–τ_1, which forms the first echo on the observer frequency, corresponds to a two-pulse ESEEM experiment. By inserting a subsequence $\pi/2(\nu_A)$–t_{store}–$\pi/2(\nu_A)$ at the time of first echo formation the transverse magnetization would be stored along z and the whole observer pulse sequence would correspond to the remote echo detected two-pulse ESEEM experiment [27]. The pump pulse could then be applied during the

interval of length t_{store}. However, in this version of the experiment at least half the magnetization would not be stored but lost. Therefore, we omit the storage.

As a result, the nuclear modulation of the observer sequence as a function of τ_1 does not conform to the expressions derived for two-pulse ESEEM. However, nuclear modulation is still observed on the refocused echo. This is because at time of formation of the first echo several of the coherence transfer echoes that contribute to the two-pulse ESEEM effect consist of allowed electron coherence [28]. The major fraction of this allowed electron coherence is refocused by the last observer π pulse without conversion into forbidden coherence. This coherence transfer pathway introduces modulation of the refocused echo with nuclear frequencies ω_α and ω_β as well as with the difference combination frequency $|\omega_\alpha - \omega_\beta|$. In contrast, modulation with the sum combination frequency $|\omega_\alpha + \omega_\beta|$ in two-pulse ESEEM is solely due to detection of forbidden coherence at the time of echo formation. Simple refocusing of this forbidden coherence by the last observer π pulse would lead to a total phase of $(\tau_1 + \tau_2)(|\omega_\alpha + \omega_\beta|)$. Since τ_2 is of the order of several microseconds, it is long compared to the inverse dispersion of the sum combination frequency. Thus, in practice modulation with the sum frequency decays completely. Pathways where the last observer π pulse converts the forbidden coherence to allowed coherence lead to modulation phases $(|\omega_\alpha + \omega_\beta|)\tau_1 + \omega_\alpha\tau_2$ and $(|\omega_\alpha + \omega_\beta|)\tau_1 + \omega_\beta\tau_2$. These terms also decay completely due to the dispersion of the basic nuclear frequencies ω_α and ω_β.

This feature of the four-pulse observer sequence with variable τ_1 simplifies the modulation pattern for matrix nuclei with small hyperfine couplings. For such nuclei, the difference frequency is close to zero and is removed together with the unmodulated part by a polynomial background correction. The basic nuclear frequencies are close to the nuclear Zeeman frequency ω_I and the sum frequency is close to $2\omega_I$. While two pulse ESEEM contains contributions at both the nuclear Zeeman frequency and twice its value, the modulation of the four-pulse observer sequence contains only the contribution at ω_I.

With the usual data processing for two-dimensional ESEEM experiments [28], such an ESEEM-correlated DEER experiment would provide a two-dimensional spectrum that separates the dipolar spectra according to the frequencies of nuclei in the vicinity of the spin label. As modulation depths are usually small, this experiment is rather insensitive and thus of limited usefulness. However, deuterated spin labels or spin labels in a deuterated environment feature strong deuterium modulations, while spin labels with natural isotope abundance in a matrix with natural isotope abundance feature no deuterium modulation at all. The experiment can thus be used as a basis for discriminating between the two cases. For such a discrimination, conventional processing of two-dimensional data set $V(t, \tau_1)$ is not the method of choice. In analogy to the case of isotope selection by choice of pump and observer position, it is advantageous to extract solely the contribution of the deuterated spin label (or spin label in a deuterated environment) to the time-domain DEER data. This contribution can then be further processed by the existing techniques for data analysis of dipolar evolution functions [15].

5.2. Algorithm for nuclear modulation filtering

Extraction of the contribution of deuterated spin labels corresponds to application of a band-pass filter at the deuterium frequency. For best sensitivity, the profile of this band-pass filter should match the line width and line shape of the deuterium line. As a good approximation, we may use a Gaussian profile whose center frequency ω_D and width σ are determined by fitting the deuterium modulation of the sample. Furthermore, we treat the phase ϕ_D of the deuterium modulation as a fit parameter. This approach obviates the need for deriving an analytical expression for the nuclear modulation and avoids errors due to the deviation of the experimental modulation from such an expression.

The experimental nuclear modulation function $V_{nuc}(\tau_1)$ can be obtained by adding all traces of the two-dimensional data set that differ in their t value (sum projection along the t dimension) and subtracting an exponential decay or a polynomial as the background function. This function is then fitted by the inverse Fourier transform $f(\tau_1)$ of the filter function $F(\omega)$. We use

$$f(\tau_1) = \exp\left\{-\left(\frac{t}{\sigma}\right)^2\right\}\cos(\omega_D t + \phi_D). \tag{8}$$

The contribution due to deuterated spin labels is then given by filtering the original two-dimensional data set $V(t, \tau_1)$ in the ESEEM dimension while at the same time computing the projection onto the DEER dimension:

$$V_D(t) = \int f(\tau_1)V(t, \tau_1)\,d\tau_1. \tag{9}$$

In practice, summation over all data points in the τ_1 dimension substitutes for the integration. This procedure corresponds to application of a Gaussian apodization function and subsequent extraction of the Fourier component at the deuterium frequency with proper phase correction.

5.3. Experimental result

The two-dimensional ESEEM-correlated DEER experiment was performed on a mixture of biradical **1** with deuterated nitroxide labels with biradical **2** with natural abundance nitroxide labels in a natural abundance *o*-terphenyl matrix. The sum projection along the t dimension (dotted line in Fig. 8A) features a strong deuterium modulation (initial modulation depth of 19%) and a moderate proton modulation. As the modulation decays rather fast, data were measured only up to $\tau_1 = 2.2\ \mu s$. On that time scale, the background decay can be fitted either by an exponential decay or by a low-order polynomial. We use an exponential decay function (dashed line). After subtracting

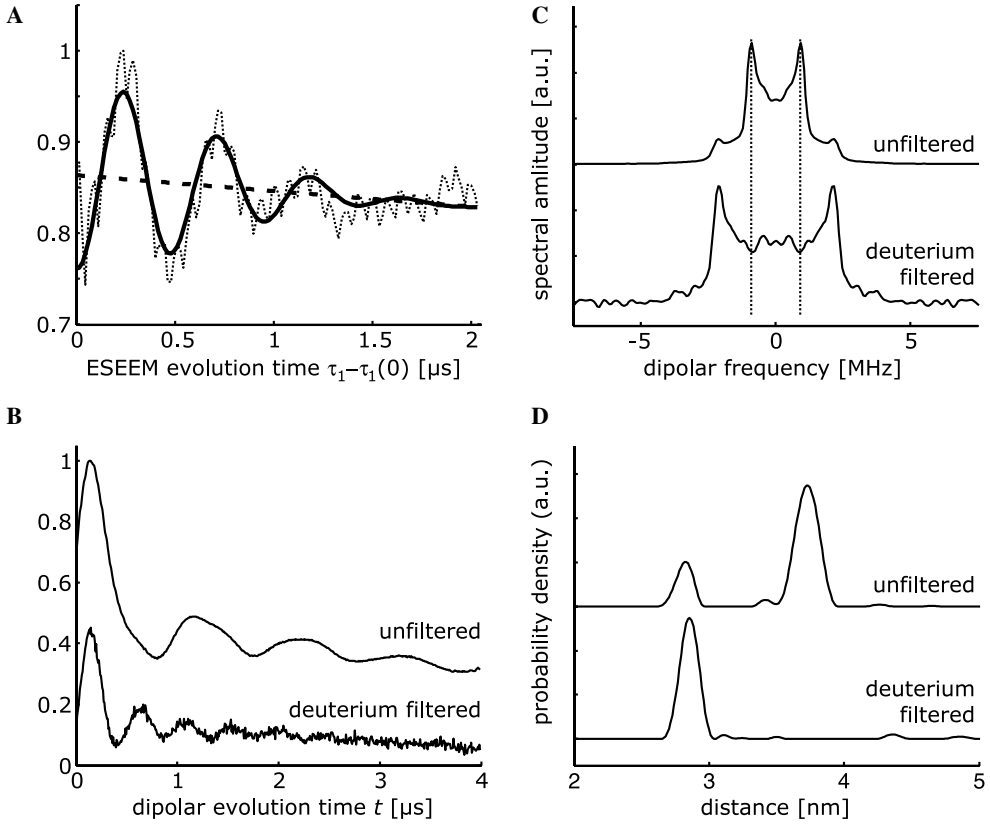

Fig. 8. Nuclear modulation filtered DEER. (A) Sum projection of the two-dimensional data set $V(t,\tau_1)$ along the t dimension (dotted line), background fit by an exponential decay (dashed line), and sum of the background function and the filter function $f(t)$ (solid line). (B) Unfiltered sum projection of the data set $V(t,\tau_1)$ along the τ_1 dimension (top trace) and deuterium-filtered sum projection (bottom trace). (C) Dipolar spectra corresponding to the unfiltered (top) and deuterium filtered (bottom) time-domain DEER data. (D) Distance distributions corresponding to the unfiltered (top) and deuterium filtered (bottom) time-domain DEER data.

this decay the filter function $f(\tau_1)$ corresponding to Eq. (8) was fitted. The sum of $f(\tau_1)$ and the decay function is shown as a solid line. Applying this filter to the data leads to a significant decrease in signal-to-noise ratio compared to the unfiltered DEER trace (Fig. 8B), which is only partially due to suppression of the component corresponding to biradical **2**. The main loss in signal-to-noise ratio results from the fact that the modulation depth is much smaller than unity even for deuterated labels.

The loss in signal-to-noise ratio is also clearly visible in the dipolar spectra (Fig. 8C). On the other hand, suppression of the contribution from biradical **2** is complete: no peaks are observed in the filtered spectrum at the position of the singularities of the spectrum of this biradical (dotted lines). Likewise, no contribution from biradical **2** is detected in the distance distribution obtained by Tikhonov regularization (Fig. 8D). In particular for materials science applications, where sensitivity of DEER is often not the limiting factor, this experiment may thus be valuable for simplifying distance distributions. Application to biomacromolecules may also be feasible, even in frozen aqueous solution with shorter relaxation times of the electron spins, since sensitivity can be strongly improved by reducing τ_2 and the maximum value of τ_1 for systems with broader distance distributions.

6. Conclusion

Selective distance measurements that discriminate between isotope-labeled nitroxides and nitroxides with natural isotope abundance can be performed by combining ^{15}N labelling with a variation of the pump and observer position or by combining deuteration of labels with nuclear modulation filtering. The former approach has better sensitivity, while the latter approach leads to a more complete suppression of the unwanted contribution. Future application of such techniques may encounter more complex systems, which do not consist exclusively of isotopically bilabeled and unlabeled pairs, but may also contain monolabeled pairs. The methodology developed so far can then still simplify the distance distributions, but may not completely unravel all contributions. Work on an extension of the approach to such problems is now under progress.

References

[1] A.D. Milov, K.M. Salikhov, M.D. Shirov, Application of ELDOR in electron-spin echo for paramagnetic center space distributions in solids, Fiz. Tverd. Tela (Leningrad) 23 (1981) 957–982.

[2] A.D. Milov, A.B. Ponomarev, Yu.D. Tsvetkov, Electron–electron double-resonance in electron-spin echo: model biradical systems and the sensitized photolysis of decalin, Chem. Phys. Lett. 110 (1984) 67–72.
[3] V.V. Kurshev, A.M. Raitsimring, Yu.D. Tsvetkov, Selection of dipolar interaction by the 2+1 pulse train ESE, J. Magn. Reson. 81 (1989) 441–454.
[4] P.P. Borbat, J.H. Freed, Multiple-quantum ESR and distance measurements, Chem. Phys. Lett. 313 (1999) 145–154.
[5] M. Pannier, S. Veit, A. Godt, G. Jeschke, H.W. Spiess, Dead-time free measurement of dipole–dipole interactions between electron spins, J. Magn. Reson. 142 (2000) 331–340.
[6] G. Jeschke, M. Pannier, A. Godt, H.W. Spiess, Dipolar spectroscopy and spin alignment in electron paramagnetic resonance, Chem. Phys. Lett. 331 (2000) 243–252.
[7] G. Jeschke, A. Bender, H. Paulsen, H. Zimmermann, A. Godt, Sensitivity enhancement in pulse EPR distance measurements, J. Magn. Reson. 169 (2004) 1–12.
[8] L.J. Berliner, S.S. Eaton, G.R. Eaton (Eds.), Biological Magnetic Resonance, vol. 19, Plenum, New York, 2000.
[9] L. Columbus, W.L. Hubbell, A new spin on protein dynamics, Trends Biochem. Sci. 27 (2002) 288–295.
[10] H.J. Steinhoff, B. Suess, Molecular mechanisms of gene regulation studied by site-directed spin labeling, Methods 29 (2003) 188–195.
[11] P. Fajer, Site directed spin labelling and pulsed dipolar electron paramagnetic resonance (double electron–electron resonance) of force activation in muscle, J. Phys.: Condens. Mat. 17 (2005) S1459–S1469.
[12] A.D. Milov, A.G. Maryasov, Yu.D. Tsvetkov, Pulsed electron double resonance (PELDOR) and its applications in free-radicals research, Appl. Magn. Reson. 15 (1998) 107–143.
[13] G. Jeschke, Determination of the nanostructure of polymer materials by electron paramagnetic resonance spectroscopy, Macromol. Rapid Commun. 23 (2002) 227–246.
[14] G. Jeschke, A. Koch, U. Jonas, A. Godt, Direct conversion of EPR dipolar time evolution data to distance distributions, J. Magn. Reson. 155 (2002) 72–82.
[15] G. Jeschke, G. Panek, A. Godt, A. Bender, H. Paulsen, Data analysis procedures for pulse ELDOR measurements of broad distance distributions, Appl. Magn. Reson. 26 (2004) 223–244.
[16] M.K. Bowman, A.G. Maryasov, N. Kim, V.J. DeRose, Visualization of distance distribution from pulsed double electron–electron resonance data, Appl. Magn. Reson. 26 (2004) 23–39.
[17] Y.W. Chiang, P.P. Borbat, J.H. Freed, The determination of pair distance distributions by pulsed ESR using Tikhonov regularization, J. Magn. Reson. 26 (2005) 279–295.
[18] G. Jeschke, A. Bender, T. Schweikardt, G. Panek, H. Decker, H. Paulsen, Localization of the N-terminal domain in light-harvesting chlorophyll a/b protein by EPR measurements, J. Biol. Chem. 280 (2005) 18623–18630.
[19] G. Jeschke, A. Godt, Co-conformational distribution of nanosized [2] catenanes determined by pulse EPR measurements, ChemPhysChem 4 (2003) 1328–1334.
[20] D. Hilger, H. Jung, E. Padan, C. Wegener, K.-P. Vogel, H.-J. Steinhoff, G. Jeschke, Assessing oligomerization of membrane proteins by four-pulse DEER: pH-dependent dimerization of NhaA Na^+/H^+ antiporter of *E-coli*, Biophys. J. 89 (2005) 1328–1338.
[21] A.M. Lesk, Introduction to Protein Science, Oxford University Press, Oxford, 2004.
[22] G. Jeschke, Distance measurements in the nanometer range by pulse EPR, ChemPhysChem 3 (2002) 927–932.
[23] E. Narr, A. Godt, G. Jeschke, Selective measurements of a nitroxide–nitroxide separation of 5 nm and a nitroxide–copper separation of 2.5 nm in a terpyridine-based copper(II) complex by pulse EPR spectroscopy, Angew. Chem., Int. Ed. 41 (2002) 3907–3910.
[24] A. Godt, C. Franzen, S. Veit, V. Enkelmann, M. Pannier, G. Jeschke, EPR probes with well-defined, long distances between two or three unpaired electrons, J. Org. Chem. 65 (2000) 7575–7582.
[25] Available at <http://www.mpip-mainz.mpg.de/~jeschke/distances.html>.
[26] P.P. Borbat, J.H. Freed, Double-quantum ESR and distance measurements, in: L.J. Berliner, G.R. Eaton, S.S. Eaton (Eds.), Biological Magnetic Resonance, vol. 19, Kluwer, New York, 2000, pp. 383–459.
[27] H. Cho, S. Pfenninger, C. Gemperle, A. Schweiger, R.R. Ernst, Zero deadtime pulsed ESR by remote echo detection, Chem. Phys. Lett. 160 (1989) 391–395.
[28] A. Schweiger, G. Jeschke, Principles of Pulse Electron Paramagnetic Resonance, Oxford University Press, Oxford, 2001.